Kinetic Description of Structural Changes Linked to Membrane Import of the Colicin E1 Channel Protein†

Stanislav D. Zakharov,‡,§ Magdalen Lindeberg,‡ and William A. Cramer*,‡

Department of Biological Sciences, Purdue University, West Lafayette, Indiana 47907-1392, and Institute of Basic Biological Problems, Russian Academy of Sciences, Pushchino, Moscow Region, Russia

Received February 9, 1999; Revised Manuscript Received May 13, 1999

ABSTRACT: Upon binding to membranes, the 178-residue colicin E1 C-terminal channel protein forms a steady-state closed-channel intermediate that is a flexible extended two-dimensional helical array [Zakharov et al. (1998) *Proc. Natl. Acad. Sci. U.S.A. 95*, 4282−4287]. Analysis of the kinetics of binding−insertion to liposome membranes of the channel protein, P178, and of changes of spectral parameters associated with structure transitions allowed a correlation of the sequence of tertiary and secondary structure changes with binding−insertion. Binding and insertion were distinguished by use of lipids modified with quenchers of Trp fluorescence attached to lipid headgroups or acyl chains. Secondary and tertiary structure changes were inferred, respectively, from changes in far-UV circular dichroism and relative changes of interresidue distances by fluorescence resonance energy transfer (FRET). "Single Trp" mutants were used in FRET analysis, with the background Tyr contribution determined through use of a "zero Trp" mutant. The sequence of distinguishable events and the pseudo-first-order rate constants under "standard" conditions (large unilamellar vesicles, pH 4.0, $I = 0.1$ M) was binding (30 ± 5 s^{-1}) → unfolding (12.6 ± 0.5 s^{-1}) → helix elongation (9.0 ± 1.0 s^{-1}) → insertion (6.6 ± 0.5 s^{-1}). Thus, helix elongation on the surface of the membrane can occur after unfolding and does not require insertion. Binding−insertion and structural transitions of P178 occur significantly faster with small unilamellar vesicles. The relevance to general mechanisms of protein import of the structural changes associated with import of the colicin channel is discussed.

The colicins are a group of plasmid-encoded proteins produced by *Escherichia coli* and related bacteria.[1] They are targeted against related strains that do not possess the plasmid coding for colicin immunity. The bactericidal function of pore-forming colicins is associated with their ability to form a highly conductive ion channel in the bacterial cytoplasmic membrane (for reviews, see refs *1*−*3*).

The water-soluble C-terminal channel-forming domain of colicin E1 is a compactly packed globule with a well-developed core formed by hydrophobic helices 8 and 9 and their contacts with nonpolar side chains of hydrophilic and amphipathic helices (*4*). This state is characterized by a blue-shifted maximum (∼327 nm) of tryptophan fluorescence, strong near-UV CD signals, ca. 70% helical content, and a partial specific heat capacity of 37 kJ mol^{-1} K^{-1} (*5*). Binding of the channel domain to the membrane is associated with a large structural transition that results in the formation of an extended flexible two-dimensional helical array in the membrane interfacial layer (*5*). This membrane-bound state has the properties (lengthened helices, flexible coupling between helical segments) that are appropriate for an intermediate closed state from which the open channel can be formed by imposition of a electrical membrane potential (*6*).

Membrane binding does not greatly affect the position of the maximum in the spectrum of Trp fluorescence but leads to a loss of the near-UV CD signals from aromatic side chains. This implies that all three tryptophans are in a nonpolar environment in the membrane-bound (P_m) as well as in the water-soluble (P_s) state, but their position is not constrained by interhelix interactions in P_m. Weaker and less extensive interhelix contacts, and much higher helicity (ca. 85%), of an expanded 2D helical array in the interfacial layer of membrane bilayer were inferred from differential scanning calorimetry, CD and IR spectroscopies, surface plasmon resonance, and fluorescence resonance energy transfer (*5*). The whole helical array, perhaps with the exception of the region proximal to the N-terminus, is buried in the interfacial layer and the hydrophobic membrane core. The 15.4 kDa C-terminal segment of the channel domain is inaccessible to proteases in the membrane-bound state (*7*), and the Trp

† This study was supported by NIH Grants GM-18457 (W.A.C.) and an NIH postdoctoral fellowship GM118078 (M.L.).

* To whom correspondence should be addressed: phone 765-494-4956; fax 765-496-1189; e-mail wac@bilbo.bio.purdue.edu.

‡ Purdue University.

§ Russian Academy of Sciences.

[1] Abbreviations: CD, circular dichroism; DS- and DOPC, 1,2-distearoyl- and 1,2-dioleoylphosphatidylcholine; DS- and DOPG, 1,2-distearoyl- and 1,2-dioleoylphosphatidylglycerol; *E*, efficiency of energy transfer; ϵ, dielectric constant; F_{290} and F_{337}, fluorescence at 490 nm excited at 290 or 337 nm; FRET, fluorescence resonance energy transfer; *I*, ionic strength; IAEDANS, 5-[[[(2-iodoacetyl)amino]ethyl]-amino]naphthalene-1-sulfonic acid; λ_{em} and λ_{ex}, emission and excitation wavelengths; L(S)UV, large (small) unilamellar vesicles; P178 and P190, C-terminal channel polypeptides of colicin E1; P_s and P_m, soluble and membrane-bound protein (P178); *R*, distance between W396 and 509C−AEDANS in P178; [Θ], molar ellipticity per residue; TNP-PE, *N*-(trinitrophenyl)phosphatidylethanolamine; UV, ultraviolet.

10.1021/bi9903087 CCC: $18.00
Published on Web 08/13/1999

residues are positioned 6−10 Å from the bilayer center (*8*).

The binding of the colicin channel domain to membranes in vitro at acidic pH is driven by electrostatic interactions between the positively charged regions of the protein and the anionic membrane surface (*9*, *10*). Therefore, the rate of the protein transition from the soluble to the membrane-bound state is strongly pH- and ionic strength-dependent (*9*). In the present study, kinetic analysis of changes of spectral parameters associated with membrane binding, unfolding of tertiary structure, elongation of surface-bound helices, and insertion allowed a description of the sequence of events associated with formation of the initial membrane-bound closed channel intermediate of the colicin E1 channel domain. The structure changes that occur to the channel domain upon membrane binding would appear to facilitate the voltage-dependent transition to the open-channel state, which involves formation of additional transmembrane helices (*5*).

MATERIALS AND METHODS

Colicin E1 Channel Polypeptide. The 178 residue C-terminal colicin E1 channel polypeptide, P178, was prepared by thermolysin proteolysis of intact colicin E1 (*11*). The wild-type polypeptide with three tryptophans at positions 424, 460, and 495, nine tyrosines, and a single cysteine at 505, buried in the protein globule in the native state, was used in Trp fluorescence quenching and CD experiments. Single Trp, W396, and "zero Trp" mutants with a solvent-exposed cysteine at position 509 were used in FRET experiments. The Y396W mutant was constructed in a "zero Trp" mutant W424F/W460F/W495F (*12*) by the PCR-based megaprimer method (*13*) and linked to D509C by replacing the *Sma*I−*Eco*RI fragment in pT7E1C505A/D509C with the same fragment from the single Trp mutant. The pT7E1C505A/D509C mutant was created by PCR amplification of the *Eco*RI−*Bam*HI fragment from a C505A mutant with D509C encoded by the upstream primer.

Unilamellar Lipid Vesicles. Large unilamellar vesicles (LUV) equivalent to 20 mM phospholipids were prepared from DOPG and DOPC (Avanti Polar Lipids, Alabaster, AL) in a 2:3 molar ratio by extrusion through a 0.1 μm pore size filter (Nucleopore, Costar, Cambridge, MA), as previously described (*9*, *14*). DOPG and Br_4(9,10)-DSPC (Avanti) or TNP-PE (Sigma), DOPG, and DOPC in molar ratio 2:3 or 1:8:11, respectively, were used in tryptophan quenching experiments. SUV were prepared by sonication of the respective lipid mixture with an ultrasonic bath-type disintegrator. All liposomes were prepared in 20 mM Na/H-acetate and 0.1 M NaCl, pH 4.0.

Conditions for Kinetic Measurements. All rate constants were obtained under the following standard conditions, unless otherwise mentioned: concentrations of protein (P178) and liposomes (equivalent to total lipid concentration) in final mixture, 0.5 and 250 μM, respectively; 40 mol % anionic lipid (DOPG); temperature, 25 °C. Buffer was 20 mM Na/H-acetate and 0.1 M NaCl (pH 4.0, $I = 0.104$ M).

Stopped-Flow Fluorometry. A stopped-flow spectrofluorometer SX.18MV (Applied Photophysics, Leatherhead, U.K.) with monochromators in both the excitation and emission beams was used for the recording of the kinetics of (i) quenching of Trp fluorescence ($\lambda_{ex} = 290$ nm; $\lambda_{em} = 340$ nm; band-pass, 10 nm); (ii) FRET from W396 to 509C−AEDANS ($\lambda_{ex} = 290$ nm; $\lambda_{em} = 490$ nm; band-pass, 10 and 25 nm, respectively). The dead time of the instrument (ca.1.5 ms) was verified by reduction of the dye dichlorophenolindophenol by ascorbic acid (*15*). A logarithmic time scale was used for data collection with 1000 data points accumulated in 10 s. This allowed collection of more data at short times and a more accurate determination of larger rate constants ($k > 10$ s^{-1}). One hundred microliters of each solution was mixed per mixing "shot" in the conventional stopped-flow mixing. Data were analyzed by using equations with exponential term(s) and a floating end point:

$$F_t = A\, e^{(-kt)} + B \qquad (1)$$

where A and B are the amplitude of the initial signal change and the end point value, respectively, and k is the pseudo-first-order rate constant. The fits with a single-exponential term ("pseudo-first-order") were satisfactory (correlation coefficients > 0.9) for the kinetic data for FRET, far-UV CD, and the fluorescence quenching by Br. The fit to the kinetic data for the quenching by TNP required the use of two exponential terms.

Stopped-Flow CD Spectroscopy. A Jasco-600 spectropolarimeter with a stopped-flow accessory SFC-5C, equipped with an optical cell of 1 cm path length, was used for the stopped-flow CD measurements. The parameters of the measurements were as follows: λ, 225 nm; band-pass, ≈2.5 nm; time constant, 1−4 ms; data collection interval, 1 ms. The minimum mixing dead time of the accessory, stated by the manufacturer, is ≥2 ms, and the dead volume = 70 μL. Aliquots (200 μL) of each solution, 1 μM P178 and 0.5 mM LUV, were mixed under a pressure of 80 psi and a flow time = 100 ms. The data from 30−40 mixing events were averaged and analyzed by use of eq 1. The time scan of absorbance, made simultaneously with the record of the CD signal, showed that the initial increase in light scattering upon membrane binding does not change the absorbance to a level that would impair measurement of the CD signal. The kinetics of the absorbance change were similar to that of light scattering measured at 400 nm on the stopped-flow fluorometer (data not shown).

Fluorescence Resonance Energy Transfer. Single Trp (W396) and "zero Trp" P178 mutants both containing solvent-exposed C509 were used in FRET analysis with the sulfhydryl-reactive fluorophore AEDANS attached to C509 according to refs *16* and *17*. It was not necessary to use 8 M urea to increase the accessibility of C509 because its side chain is apparently accessible, as predicted from the atomic structure (*4*), allowing its reaction with IAEDANS to be conducted under native conditions. Extinction coefficients of 1.8×10^4 M^{-1} cm^{-1}, 1.3×10^4 M^{-1} cm^{-1} at 278 nm, and 5.7×10^3 M^{-1} cm^{-1} at 337 nm were used for determination of the W396, "zero Trp", and AEDANS concentrations, respectively. Determination of the value of donor−acceptor (Trp−AEDANS) FRET efficiencies and the calculation of donor−acceptor distances employed the relationship between the donor−acceptor distance, R, efficiency for energy transfer, E, and the characteristic distance, R_0, for which the transfer efficiency is 50%:

$$R = R_0\,(E^{-1} - 1)^{1/6} \qquad (2)$$

The efficiency of transfer from W396 to AEDANS, E, was estimated from the ratio of fluorescence intensity of AEDANS at 490 nm, excited at 290 and 337 nm, respectively. Optical densities at 290 and 337 nm were <0.05. To correct for the possible involvement of tyrosines in the energy transfer and direct excitation of AEDANS at 290 nm, the fluorescence at 490 nm (λ_{ex}, 290 nm) and extinction at 290 nm of the "zero Trp"−AEDANS adduct were subtracted from the respective values of W396−AEDANS adduct:

$$E = (\Delta F_{290}/F_{337})(\epsilon_{337}/\Delta\epsilon_{290}) \quad (3)$$

where

$$\Delta F_{290} = F_{290}(\text{W396}) - F_{290}(\text{zeroW}) \quad (4)$$

$$\Delta\epsilon_{290} = \epsilon_{290}(\text{W396}) - \epsilon_{290}(\text{zeroW}) \quad (5)$$

R_0 was calculated as in ref *19*:

$$R_0 = (9.7 \times 10^3)(J\,\kappa^2\,\Delta Q n^{-4})^{1/6} \quad (6)$$

where J is the overlap integral between Trp emission spectra and the absorbance of C509−AEDANS, κ^2 and n are the orientation factor and the refractive index, respectively, and ΔQ is the quantum yield of the donor (Trp) fluorescence in the absence of energy transfer acceptor, corrected for the contribution of Tyr fluorescence:

$$\Delta Q = Q_{\text{W396}} - Q_{\text{zeroW}} \quad (7)$$

The kinetics of changes in the overlap integral (J) between Trp emission spectra and the absorbance of C509−AEDANS were measured after stopped-flow mixing, where J is described by

$$J = \int \Delta F(\lambda)\,\epsilon_{\text{AEDANS}}(\lambda)\,\lambda^4\,d\lambda / \int \Delta F(\lambda)\,d\lambda \quad (8)$$

where $\Delta F(\lambda)$ is the difference in fluorescence intensity (λ_{ex} = 290 nm) between the W396 P178 and "zero Trp" P178 proteins and $\epsilon_{\text{AEDANS}}(\lambda)$ is the molar extinction coefficient of AEDANS−P178 adduct at wavelength λ, respectively. The overlap integral was measured by using the values of $\Delta F(\lambda)$ in the spectral range 315−345 nm, measured at 5 nm intervals.

Residue 396 was chosen as the donor because it is on the surface of the protein, which should allow relatively free motion of the side chain. The absence of quenching of AEDANS fluorescence by Br-lipid (data are not shown) implied that the AEDANS moiety is not inserted into the bilayer. Therefore, free motion of AEDANS and a corresponding orientation factor of $^2/_3$ for random orientation of donor/acceptor were assumed. An important aspect of the FRET measurements in the present study is that the calculated distances could be calibrated relative to the known interresidue distance in $P178_s$ at $t = 0$. The donor−acceptor distance was assumed to be 17 Å, the distance between the CZ atom of Y396 and the OD1−OD2 atoms of D509 in the wild-type structure (*4*). In the present work, the data for interresidue distance changes were normalized for the value at $t = 0$, because it was necessary to consider only relative values of R and R_0. The new aspects of FRET analysis described above, correction for Tyr contribution, measurement of time-dependent changes in overlap integral, and the use of atomic structure data to calibrate distance values and their changes were developed in a study on the unfolding pathway of the colicin channel protein (M. Lindeberg et al., manuscript in preparation).

Determination of Standard Deviations in the Kinetic Measurements. For Trp fluorescence, light scattering, and FRET, the contribution of the noise from an individual measurement to the standard deviation of the resulting rate constants was generally smaller than that from the variations that resulted from different preparations of the proteins and especially of liposomes. For stopped-flow CD, the major component in the standard deviation was the signal-to-noise ratio for an individual measurement. Some 30−40 individual stopped-flow measurements were averaged in CD and FRET analysis, compared to 11−15 for fluorescence quenching. The errors in the rate constant determinations for all measurements except CD were decreased through the use of a logarithmic time scale of data point accumulation, as noted above, with an initial step of 10 μs. Thus, the data accumulation was more "fine-grained" at the shorter times, where the intrinsic errors are greatest.

Protein and Lipid Determination. The protein concentration of wild-type P178 samples was determined by using an extinction coefficient of $3.05 \times 10^4\ M^{-1}\ cm^{-1}$ at 279.5 nm (*5*), which was verified by a "micro" method for determination of nitrogen content (*20*). The absorbance of $P178_m$ at 279.5 nm was corrected for suspension turbidity as in ref *21*. Lipid concentrations were measured by the "micro" method (*20*), based on a determination of P_i content in ashed samples.

RESULTS

Kinetics of Binding and Insertion

Quenching of Tryptophan Fluorescence. Fluorescence quenchers bound to the lipid headgroup region [*N*-(trinitrophenyl)phosphatidylethanolamine, $R_0 \approx 27$ Å (*10*)] or in the membrane hydrophobic core (collisional quencher, C-9,10-Br_2), were employed to analyze the relation of the kinetic steps and the membrane topography in the surface binding of the colicin E1 channel polypeptide, P178. Bromine atoms at C-9,10 are ca. 8 Å from the center of the bilayer (*22*, *23*), with a range of thermal motion of ca. 10 Å (1/e half-width of the Gaussian distribution of bromine position, 5 Å; *24*). It was assumed that quenching by TNP and Br characterize, respectively, the initial association (binding) with the membrane and insertion into the membrane bilayer. Wild-type P178, possessing three Trp and nine Tyr, was used in these experiments. It has a blue-shifted Trp fluorescence emission spectrum (λ_{max}, 327 nm) in the soluble state, whose amplitude decreases only slightly (<5%) upon binding to liposomes without quencher (DOPG/DOPC in 2:3 molar ratio) without a shift in λ_{max} of the emission spectrum.

Binding and insertion were significantly faster with SUV compared to LUV (Figure 1). Due to the limited time resolution (≥10 ms) of the CD instrumentation, complete studies of the kinetics of binding−insertion and the structure changes described below were carried out only with LUV.

Quenching by TNP-PE. TNP provides efficient quenching at a relatively low concentration of modified lipids (2−5 mol

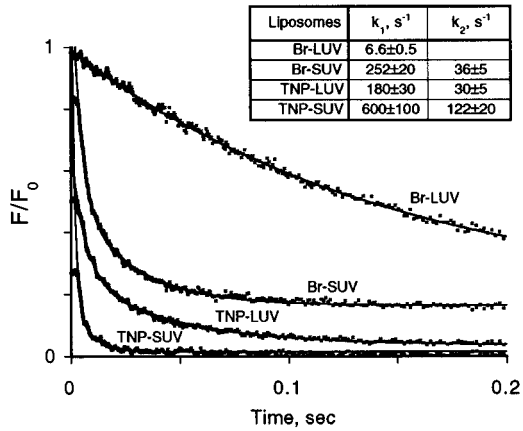

FIGURE 1: Time course of quenching of Trp fluorescence by Br or TNP upon the binding of colicin E1 P178 to liposomes; effect of liposome radius of curvature. Liposomes were prepared by extrusion through filter with 0.1 μm pores (LUV) or by sonication (SUV). Lipid content was DOPG/Br_4(9,10)-DSPC (2/3 mol/mol), for Br liposomes and DOPG/TNP-PE/DOPC (molar ratio 8/1/11) for TNP-liposomes. Final suspension contained 0.5 μM P178, 0.25 mM phospholipids in 20 mM Na/H-acetate, and 0.1 M NaCl, pH 4.0; 25 °C. All data were normalized to the unquenched level of P178 fluorescence. λ_{ex}, 290 ± 5 nm; λ_{em}, 340 ± 5 nm.

Table 1: pH and Ionic Strength Dependence of Rate Constants for P178 Binding to LUV and Insertion into Membrane Bilayer[a]

buffer		TNP-lipid		Br-lipid
pH	I (M)	k_1 (s^{-1}) [A][b]	k_2 (s^{-1})	k (s^{-1})
3.8	0.1	269 ± 50 [0.64]	38 ± 5	8.9 ± 0.5
4.0	0.1	180 ± 30 [0.60]	30 ± 5	6.6 ± 0.5
4.2	0.1	153± 30 [0.58]	14 ± 3	4.6 ± 0.3
4.4	0.1	127 ± 30 [0.29]	6 ± 2	2.1 ± 0.3
4.6	0.1	3.2 ± 0.5 [0.09]	0.13 ± 0.04	0.16 ± 0.04
4.8	0.1	0.10 ± 0.03 [0.25]	0.03 ± 0.01	0.07 ± 0.03
5.0	0.1	0.08 ± 0.03[c]		0.013 ± 0.003
4.0	0.03	222 ± 50	29 ± 5	12.5 ± 0.2
4.0	0.18	4.2 ± 0.7[c]		3.1 ± 0.2
4.0	0.28	0.15 ± 0.05[c]		0.22 ± 0.05

[a] Inferred from the quenching of Trp fluorescence by TNP (binding) or Br (insertion). [b] Fraction of amplitude of signal changes with rate constant k_1 is shown (in brackets). [c] Only one kinetic phase was detected.

%) because of its large R_0 value and is a sensitive probe for detection of membrane binding. It has been used to measure membrane binding parameters of colicin E1 C-terminal channel polypeptides and to detect reversible membrane association of soluble basic proteins such as lysozyme (*9*, *10*). In SUV or LUV, the fluorescence was quenched ≥95% with 5 mol % TNP-PE in the membrane bilayer (Figure 1). The rate of quenching was strongly pH- and ionic strength-dependent (Table 1). The data were fit best with two exponential terms. At pH 4.0 and ionic strength 0.1 M, the rate constants were $k_1 = 180 \pm 30$ s^{-1} and $k_2 = 30 \pm 5$ s^{-1}, contributing 60% and 40% to the overall kinetics, respectively. Unless otherwise stated, all rate constants refer to the above standard conditions. The magnitude of both rate constants decreased with increasing pH or ionic strength. The decrease in quenching rate was especially pronounced at pH and ionic strength values >4.5 and >0.2 M, respectively. The larger rate constant is believed to reflect the quenching that precedes actual binding and is a consequence of the large value of R_0 for TNP. This quenching originates from protein accumulation in the near-membrane space, driven by electrostatic interactions between the positively charged protein and the negative membrane surface. The smaller rate constant, $k_2 \equiv$ "k_{TNP}", is used in subsequent discussions to describe the rate of protein binding to the membrane surface. The association of k_2 with the actual binding event is also based on its similarity to the rate constant for the onset of light scattering changes arising from reversible liposome aggregation induced by colicin binding (data not shown).

Quenching by Br-Lipid. 1,2-Distearoyl(9,10-dibromo)-*sn*-glycero-3-phosphocholine (60 mol %) caused 80−90% quenching. The quenching kinetics of P178 fluorescence by Br upon binding to LUV [DOPG/Br_4(9,10)-DSPC, 2/3 mol/mol] were appreciably slower than those by TNP (Figure 1) and could be fit by a single-exponential term ($k_{Br} = 6.6 \pm 0.5$ s^{-1}), which characterizes insertion of P178 into the membrane bilayer. The rate constant for Br quenching decreased with increasing pH or ionic strength. For $3.8 \leq$ pH < 4.6, $k_{TNP} > k_{Br}$, with the disparity greater at lower pH. At pH ≥ 4.6, the binding becomes rate-limiting, and the quenching by Br and TNP (k_2) occurs with similar rate constants, $k_{Br} \approx k_{TNP} < 0.2$ s^{-1} (Table 1). As a control for the inference that Br quenching of Trp fluorescence is an indicator of protein insertion into the bilayer, Trp fluorescence of the water-soluble protein lysozyme, which binds to membranes at low pH (*9*), was not quenched by Br-lipid (data not shown).

Kinetics of Structure Changes

Far-UV Circular Dichroism Stopped-Flow Kinetics. Far-UV CD in the stopped-flow mode was used to characterize the kinetics of P178 structure changes. It is important to use the same protein and lipid concentrations in the Trp fluorescence quenching and CD measurements in order to be able to accurately correlate structure changes with membrane binding and insertion. However, optimal optical absorption for CD measurements occurs in a relatively narrow range. The presence of liposome light scattering complicates the task. Use of an optical cell with a path length of 1 cm in the stopped-flow accessory and a larger spectral bandwidth (2.5 nm) in the CD spectrometer allowed acquisition of valid kinetic data at 225 nm (Figure 2), with reasonably good spectral resolution of the negative ellipticity peak at 222 nm (Figure 2, inset). Neither TNP nor Br compromise the CD signal at 225 nm, allowing the same liposomes with modified lipids to be used in the Trp fluorescence quenching and CD measurements. The difference in kinetic parameters obtained for LUV with 60 mol % Br_4(9,10)-DSPC or DOPC was insignificant, which is not surprising, as both the DOPG/DOPC lipid mixture and Br_4-(9,10)-DSPC membranes have thermotropic phase transitions below 5 °C (*22*, *25*).

A rate constant of 9 ± 1 s^{-1} obtained upon P178 binding to LUV at pH 4.0 (Figure 2) described the kinetics of the changes from the level of the CD signal of $P178_s$ (-15 ± 1 kdeg cm^2 $dmol^{-1}$) to that of the $P178_m$ (-23 ± 2 kdeg cm^2 $dmol^{-1}$). The rate constant of the ellipticity change was weakly dependent on pH in the range 3.8−4.3 (Table 2) and declined sharply for pH values > 4.4, as did k_{TNP} and k_{Br}. A similar trend was observed in the ionic strength dependence. The rate constants were relatively independent of ionic strength for $I < 0.15$ M and decreased more rapidly for $I >$

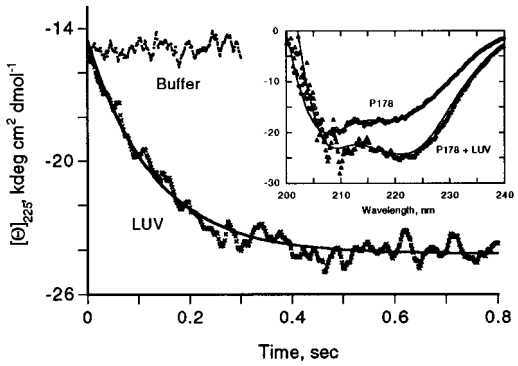

FIGURE 2: Time course of increase in α-helicity upon P178 binding to liposomes. Main panel: 1 μM P178 was mixed with LUV (0.5 mM lipids) at pH 4.0 (×). Liposomes were prepared from DOPG/Br_4-DSPC (2/3 mol/mol). Data were fit with a single exponential (solid lines). Conditions otherwise were as in Figure 1. (Inset) Spectra of $P178_s$ (○) and $P178_m$ (△), taken in a stopped-flow optical cell (path length 1 cm) after mixing with buffer or LUV (main panel) or in a cuvette with path length 0.1 mm, using 10 μM P178 and LUV equivalent to 5 mM lipids (solid lines). Jasco noise reduction program was applied to the spectra obtained in the thin cuvette only.

Table 2: pH Dependence of Increase in Helicity[a] and FRET[b] of P178 upon Binding to LUV

buffer			
pH	I (M)	$[\Theta]_{225}$ (s^{-1})	FRET (s^{-1})
3.8	0.1	9.2 ± 1.1	20.3 ± 1.8
4.0	0.1	9.0 ± 1.0	12.6 ± 0.5
4.2	0.1	7.6 ± 1.4	9.9 ± 0.5
4.4	0.1	2.8 ± 0.6	3.5 ± 0.2
4.6	0.1	0.2 ± 0.1	0.6 ± 0.2
4.8	0.1	0.02 ± 0.01	0.2 ± 0.1
4.0	0.03	9.7 ± 1.0	22 ± 1
4.0	0.18	5.8 ± 0.4	2.3 ± 0.2
4.0	0.28	0.2 ± 0.1	0.3 ± 0.1

[a] Measured by stopped-flow CD at 225 nm. [b] FRET from W396 to C509-AEDANS.

0.2 M (Table 2). Under standard conditions, k_{TNP} (30 ± 5 s^{-1}) > k_Θ (9.0 ± 1.0 s^{-1}) > k_{Br} (6.6 ± 0.5 s^{-1}). In terms of the simple membrane parameters that promote protein binding−insertion, it was of interest that the decrease of $[\Theta]_{225}$ was markedly faster for binding to SUV. At pH 4.4, where the kinetics for SUV could be resolved, k_Θ = 2.8 ± 0.6 s^{-1} and ca. 20 s^{-1} for LUV and SUV, respectively.

FRET from W396 to AEDANS−509C. FRET from a single Trp to an AEDANS-modified cysteine residue was used to study the rate of P178 tertiary structure unfolding. Tryptophan W396 belongs to helix 3 of $P190_s$ that, together with helices 4, 6, and 7, comprises part of the proposed membrane-docking face (*4*). The CZ atom of Y396 in helix 3 and the OD1 or OD2 atoms of D509 in the 9/10 loop are separated by 17 Å (Figure 3). The single Trp−single Cys (W396/C509)−AEDANS adduct was used in the FRET analysis to estimate the rate of interresidue distance changes upon binding of P178 to LUV.

The W396 in $P178_s$ has a relatively small quantum yield of fluorescence. A 7-fold increase in W396 fluorescence intensity with an emission maximum at 328 ± 2 nm occurs upon membrane binding with a rate constant of 13 s^{-1} (*18*). Therefore, the kinetics of changes in (i) efficiency of FRET and (ii) the overlap integral (W396 fluorescence vs AEDANS

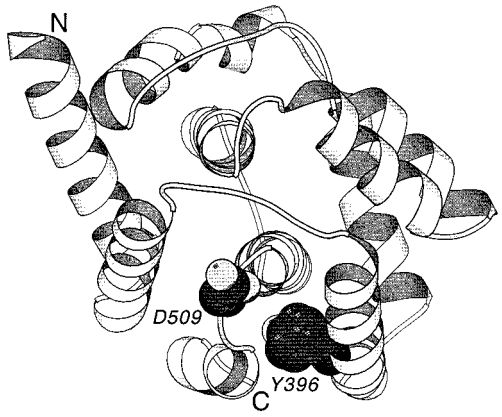

FIGURE 3: Ribbon diagram of structure of colicin E1 channel domain, $P190_s$ (*4*). Side chains of Y396 and D509 are shown.

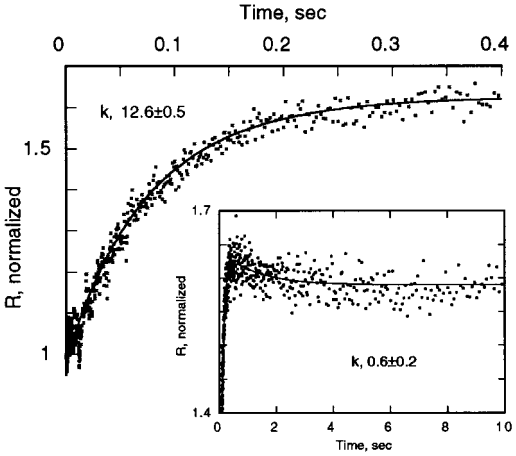

FIGURE 4: Kinetics of distance (R) change between W396 and AEDANS−C509 upon P178 binding to LUV, inferred from FRET from W396 (λ_{ex}, 290 ± 7 nm) to AEDANS (λ_{em}, 490 ± 10 nm) DOPG/DOPC (molar ratio 2:3) were used in LUV preparation. Conditions otherwise were as in Figure 1. The details of the distance calculation are described in Materials and Methods. The interresidue distance, R, calculated for P178 in the presence of membranes, is normalized to the initial distance, first data point recorded at t = 0.

light absorption), had to be carefully taken into account in the analysis (Materials and Methods). The distance between W396 and C509−AEDANS was found to increase with the pseudo-first-order rate constant, k_{FRET} = 12.6 ± 0.5 s^{-1} (Figure 4), implying that the unfolding of tertiary structure of P178 takes place simultaneously with the change in environment of Trp396. k_{FRET} was pH- and ionic strength-dependent (Table 2). k_{FRET} is larger than k_Θ at pH < 4.5 (Figure 5). Thus, considering the major distinguishable processes involved in the interaction of the colicin channel protein with the membrane, (i) surface binding, (ii) tertiary structure change = unfolding, (iii) helix elongation, and (iv) insertion, the hierarchy of the rate constants is k_{TNP} > k_{FRET} > k_Θ > k_{Br}, 3.8 < pH < 4.5 (Figure 5).

A relatively slow oppositely directed secondary phase was detected in the FRET kinetic traces (Figure 4, inset). After reaching a maximum 0.5 s after the start of the interaction, the distance between W396 and 509C−AEDANS slowly decreased with a rate constant of 0.6 ± 0.2 s^{-1} (Figure 4, inset). This effect indicates that a slow structural relaxation may occur following the initial formation of the helical two-dimensional net structure in the interfacial layer.

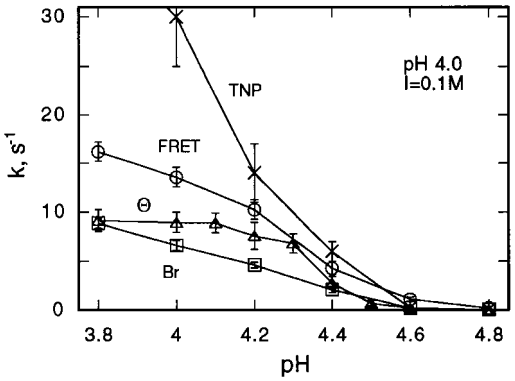

FIGURE 5: pH dependence of the rate constants for binding [k_{TNP} (×)], tertiary structure unfolding [k_{FRET} (○)], helix elongation [k_o (△)]; insertion into the membrane [k_{Br} (□)], as discussed in text. I = 0.1 M; 25 °C.

DISCUSSION

The present study provides information on the sequence of events that accompany the large structural changes associated with the transition of a toxinlike molecule from the water-soluble to a membrane-bound state. The nature of secondary and tertiary structure changes could be inferred from comparison of the kinetics of the initial electrostatic interaction and the subsequent unfolding of tertiary structure, increase in α-helicity, and insertion into the membrane bilayer, all determined under the same conditions, including the same concentrations of lipid and protein.

Kinetic Models. The pH dependence of the rates of P178 binding to the liposome membrane, measured by quenching of Trp fluorescence with lipid-attached quenchers and concomitant structure changes, shows the presence of two distinct trends associated with different rate-limiting steps in the protein structure changes that occur upon membrane binding (Figure 5). At pH values > 4.5, the rates of quenching of Trp fluorescence with TNP or Br, and of changes of FRET and of far-UV CD, are small and differences in the respective rate constants are statistically insignificant. This implies that at pH > 4.5, the structure transitions of P178 are limited by the rate of an early step, i.e., initial binding driven by the electrostatic interactions, and $k_{TNP} = k_{FRET} = k_{\Theta} = k_{Br}$.

For pH values < 4.5, the initial membrane binding is faster than the subsequent steps of protein unfolding, increase in α-helicity, and insertion into the membrane bilayer (Figure 5). Under standard conditions, the rate constants for binding, unfolding, helix elongation, and insertion are $k_{TNP} = 30 \pm 5\ s^{-1}$, $k_{FRET} = 12.6 \pm 0.5\ s^{-1}$, $k_{\Theta} = 9.0 \pm 1.0\ s^{-1}$, and $k_{Br} = 6.6 \pm 0.5\ s^{-1}$. After the approach of the colicin channel domain to the membrane and its accumulation in the near-membrane space, P_s binds to the membrane surface (P_{bound}, Figure 6). Both steps are driven by electrostatic interactions, and their rates are determined, respectively, by the larger and smaller rate constants for TNP quenching of Trp fluorescence. Encountering the membrane interfacial layer, P178 unfolds and expands on the membrane surface with the rate constant k_{FRET}. It was concluded that unfolding of the tertiary structure precedes helix elongation because (a) $k_{FRET} > k_{\Theta}$ in the pH range 3.8−4.4 (Figure 5) and (b) k_{FRET} for Trp residues inserted into other parts of the protein is similar to or larger than that for W396 (*18*). Once the activation barrier imposed by structure constraints is removed by the unfolding, helix formation is thermodynamically advantageous in the low-polarity environment ($\epsilon \sim 20$; *26*) of the membrane interfacial layer (*27*−*29*). Helix elongation is a necessary prerequisite for the formation of transmembrane helices in the open channel state, because the average length of the helices in the soluble colicin E1 channel protein is only 12 residues (*5*), whereas the length of a helix spanning the membrane bilayer should be approximately 20 residues. Thus, it is inferred that helix elongation precedes and does not require insertion into the membrane bilayer. The binding−insertion sequence of events, $P_{sol} \rightarrow P_{ins}$ (Figure 6), does not include the slow (0.5−1.0 s^{-1}) relaxation to a final steady-state conformation. The presence of some interhelix contacts in the final relaxed conformation was suggested by the partially cooperative melting of $P190_m$, detected by differential scanning calorimetry, and by temperature-dependent reversible changes in FRET at temperatures < 40 °C (*5*).

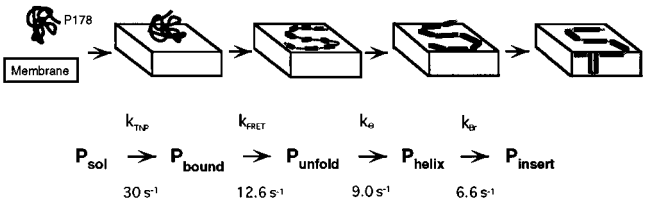

FIGURE 6: Pathway of the distinguishable structural transitions of P178 in the course of binding to the membrane surface and insertion into the membrane bilayer. Rate constants for the defined steps were measured at pH 4.0, I = 0.1 M, and 25 °C.

In a previous study on membrane interactions of the colicin A channel domain (*30*), it was concluded that the rate constants for the loss of CD signal in the near UV and Br quenching of Trp fluorescence were similar and small (ca. 0.02 s^{-1}). This may have been a result of measurements having been made at pH 5.0, where the rate for all steps is limited by the rate of initial binding to the membrane. Additional uncertainty in the comparison between fluorescence quenching and far-UV CD measurements may have resulted from the 25-fold lower concentration of colicin and liposomes used in the fluorescence compared to the CD measurements (*30*).

Comparative Kinetics of Binding−Insertion with SUV and LUV. Larger rate constants for binding, insertion, unfolding, and helix elongation were observed upon P178 binding to SUV [300−400 Å diameter (*31*)] compared to LUV [800−1200 Å diameter (*32*)] with the same anionic lipid content (Figures 1 and 2). This is presumably a result of a more facile protein insertion with SUV, which would be a consequence of greater local surface curvature, less orderly lipid packing in the outer leaflet, or an uneven distribution of lipids between outer and inner leaflets of the membrane bilayer (*33*, *34*).

Precursor State for $P178_m$ Import and Channel Formation. In the presence of a transmembrane electrical potential, the colicin ion channel is formed by a bundle of transmembrane helices (*1*), the hairpin of helices 8−9, which is inserted in the closed-channel state (*35*), and 2−4 additional helices that must be inserted into the bilayer (*6*). The flexible two-dimensional helical array in the membrane interfacial layer would facilitate a transition to the open-channel state in several ways: (i) a flexible conformation with weakly

interacting helices requires minimal energy input for conformational change; (ii) insertion of the protein into the interfacial layer of intermediate dielectric constant membrane [$\epsilon \sim 20$ (*26*)] lessens the membrane barrier associated with formation of transmembrane helices; (iii) at least some α-helices [average length 17 residues (*5*)] would become long enough to span the membrane in the presence of a membrane potential.

Synergistic Effects of Low pH and Membrane Binding Interactions on Unfolding of Tertiary Structure. P178 has 23 carboxyl groups (15 D, 7 E, C-terminus) and 27 amino groups (24 K, 2 H, R, N-terminus). The interaction of colicin with membranes in vitro requires a low pH. An increase in net positive charge of the protein after partial protonation of carboxyl groups leads to a stronger electrostatic interaction with the negatively charged membrane surface and, hence, faster membrane binding (ref *9*; Table 1), and a faster rate of unfolding (ref *16*; Table 2). However, acid destabilization of the colicin E1 channel domain in an aqueous environment is not sufficient to unfold the colicin E1 channel protein at pH > 2 (*36*). Therefore, a low pH in the near-membrane space due to the negative surface potential (ΔpH < 1 at 40 mol % anionic lipids) is not by itself a major factor in the channel domain unfolding at the membrane surface, as was proposed for the colicin A channel domain (*37*, *38*). Liposomes, containing only neutral lipid, can bind colicin, albeit slowly (*39*). Therefore, it is concluded that expansion of the colicin channel domain on the membrane surface is induced by the concerted effect of acid denaturation, electrostatic interaction of positive side chains with lipid headgroups, and nonelectrostatic interaction of protein hydrophobic sites with lipid nonpolar groups. It is important that the loss of tertiary structure takes place at the membrane surface, precluding formation of a molten globule state in solution, because exposure of the protein hydrophobic core to solvent during unfolding in an aqueous environment could result in protein aggregation.

Consequences for Generic Aspects of Protein Import. The above considerations for facilitating membrane import of the colicin channel and "gating" to the open channel state are relevant to protein import in membrane biogenesis. Protein unfolding is a prerequisite for import in membrane biogenesis (*40*). An unfolded flexible state, which can facilitate insertion of the protein into the membrane, may be an inevitable consequence of the surface-bound precursor state. Many properties of this state can be inferred from studies with liposomes. Generalizations made from studies on protein interaction with liposomes could be criticized because protein import is well-known to require many protein cofactors. However, some functions of these cofactors, decreasing electrostatic or energetic barriers, may be bypassed by using "optimized" conditions with liposomes (e.g., low pH instead of an acid chain of increasing affinity; ref *41*). Furthermore, general properties of membrane protein topology, e.g., the basis of the *cis*-positive rule for topology of membrane proteins (*42*), can be understood only from consideration of the ubiquitous anionic surface potential of the lipid in membranes (*43*).

ACKNOWLEDGMENT

We thank K. Takahashi of the Kyowa Hakko Kogyo Co. Ltd., Japan, for a kind gift of mitomycin C and J. Hollister and C. Greski for expert help in the completion of the manuscript.

REFERENCES

1. Cramer, W. A., Heymann, J. B., Schendel, S. L., Deriy, B. N., Cohen, F. S., Elkins P. A., and Stauffacher, C. V. (1995) *Annu. Rev. Biophys. Biomol. Struct. 24*, 611−641.
2. Lazdunski, C. J., Bouveret, E., Rigal, A., Journet, L., Lloubes, R., and Benedetti, H. (1998) *J. Bacteriol. 180*, 4993−5002.
3. Stroud, R. M., Reiling, K., Wiener, M., and Freymann, D. (1998) *Curr. Opin. Struct. Biol. 8*, 525−533.
4. Elkins, P. A., Bunker, A., Cramer, W. A., and Stauffacher, C. V. (1997) *Structure 5*, 443−458.
5. Zakharov, D. S., Lindeberg, M., Griko, Y., Salamon, Z., Tollin, G., Prendergast, F. G., and Cramer, W. A. (1998) *Proc. Natl. Acad. Sci. U.S.A. 95*, 4282−4287.
6. Qiu, X.-Q., Jakes, K. S., Kienker, P. K., Finkelstein, A., and Slatin, S. L. (1996) *J. Gen. Physiol. 107*, 313−328.
7. Zhang, Y.-L., and Cramer, W. A. (1992) *Protein Sci. 1*, 1666−1676.
8. Palmer, L. R., and Merrill, A. R. (1994) *J. Biol. Chem. 269*, 4187−4193.
9. Zakharov, S. D., Heymann, J. B., Zhang, Y.-L., and Cramer, W. A. (1996) *Biophys. J. 70*, 2774−2783.
10. Heymann, J. B., Zakharov, S. D., Zhang, Y.-L., and Cramer, W. A. (1996) *Biochemistry 35*, 2717−2725.
11. Bishop, L. J., Bjes, E. S., Davidson, V. L., and Cramer, W. A. (1985) *J. Bacteriol. 164*, 237−244.
12. Merrill, A. R., and Cramer, W. A. (1990) *Biochemistry 29*, 8529−8534.
13. Barik, S. (1995) *Mol. Biotechnol. 3*, 1−7.
14. Hope, M. J., Bally, M. B., Webb, G., and Cullis, P. R. (1985) *Biochim. Biophys. Acta 812*, 55−65.
15. Tonomura, B., Nakatani, H., Ohnishi, M., Yamaguchi-Ito, J., and Hiromi, K. (1978) *Anal. Biochem. 84*, 370−383.
16. Merrill, A. R., Cohen, F. S., and Cramer, W. A. (1990) *Biochemistry 29*, 5829−5836.
17. Steer, B. A., and Merrill, A. R. (1994) *Biochemistry 33*, 1108−1115.
18. Deleted in proof.
19. Förster, T. (1959) *Discuss. Faraday Soc. 27*, 7−17.
20. Jaenicke, L. (1974) *Anal. Biochem. 61*, 623−627.
21. Venyaminov, S. Y., and Gogia, Z. V. (1982) *Eur. J. Biochem. 126*, 299−309.
22. McIntosh, T. J., and Holloway, P. W. (1987) *Biochemistry 26*, 1783−1788.
23. Bolen, E. J., and Holloway, P. W. (1990) *Biochemistry 29*, 9638−9643.
24. Wiener, M. C., and White, S. H. (1991) *Biochemistry 30*, 6997−7008.
25. Silvius, J. R. (1982) in *Lipid−Protein Interactions* (Jost, P. C., and Griffith, O. H., Eds.) Vol. 2, pp 239−281, J. Wiley & Sons, Inc., New York.
26. Raudino, A., and Mauzerall, D. (1986) *Biophys. J. 50*, 441−449.
27. Wattenbarger, M. R., Chan, H. S., Evans, D. F., Bloomfield, V. A., and Dill, K. A. (1991) *J. Chem. Phys. 93*, 8343−8351.
28. Engelman, D. M., and Steitz, T. A. (1981) *Cell 23*, 411−422.
29. Jacobs, R. E., and White, S. H. (1989) *Biochemistry 28*, 3421−3437.
30. Evans, L. J. A., Goble, M. L., Hales, K. A., and Lakey, J. H. (1996) *Biochemistry 35*, 13180−13185.
31. Mayhew, E., Lazo, R., and Vail, W. J. (1984) in *Liposome Technology* (Gregoriadis, G., Ed.) Vol. II, pp 19−31, CRC Press, Inc., Boca Raton, FL.
32. Mayer, L. D., Hope, M. J., and Cullis, P. R. (1986) *Biochim. Biophys. Acta 858*, 161−168.
33. Huang, C., and Mason, J. T. (1978) *Proc. Natl. Acad. Sci. U.S.A. 75*, 308−310.
34. Gruner, S. M. (1991) in *Biomembrane Electrochemistry* (Blank, M., and Vodyanov, I., Eds.) pp 129−149, American Chemical Society, Washington, DC.

35. Kim, Y., Valentine, K., Opella, S. J., Schendel, S. L., and Cramer, W. A. (1998) *Protein Sci. 7*, 342−348.
36. Schendel, S. L., and Cramer, W. A. (1994) *Protein Sci. 3*, 2272−2279.
37. Van der Goot, F. G., Gonzalez-Mañas, J. M., Lakey, J. H., and Pattus, F. (1991) *Nature 354*, 408−410.
38. Gonzalez-Manas, J. M., Lakey, J. H., and Pattus, F. (1992) *Biochemistry 31*, 7294−7300.
39. Shin, Y.-K., Levinthal, C., Levinthal, F., and Hubbell, W. L. (1993) *Science 259*, 960−963.
40. Eilers, M., Hwang, S., and Schatz, G. (1988) *EMBO J. 7*, 1139−1145.
41. Komiya, T., Rospert, S., Koehler, C., Looser, R., and Schatz, G. (1998) *EMBO J. 17*, 3886−3898.
42. von Heijne, G. (1986) *EMBO J. 5*, 3021−3027.
43. Krishtalik, L. I., and Cramer, W. A. (1995) *FEBS Lett. 369*, 140−143.

BI9903087